



ELSEVIER

Contents lists available at SciVerse ScienceDirect

Planetary and Space Science

journal homepage: www.elsevier.com/locate/pss

SAR interferometry at Venus for topography and change detection

Franz J. Meyer^{a,b,*}, David T. Sandwell^c^a Geophysical Institute, University of Alaska Fairbanks, Fairbanks, AK 99775, USA^b Alaska Satellite Facility, University of Alaska Fairbanks, Fairbanks, AK 99775, USA^c Scripps Institute of Oceanography, University of California San Diego, CA 92093, USA

ARTICLE INFO

Article history:

Received 1 March 2012

Received in revised form

4 October 2012

Accepted 5 October 2012

Keywords:

Venus

Topography

Mapping

SAR interferometry

Remote sensing

ABSTRACT

Since the Magellan radar mapping of Venus in the early 1990's, techniques of synthetic aperture radar interferometry (InSAR) have become the standard approach to mapping topography and topographic change on Earth. Here we investigate a hypothetical radar mission to Venus that exploits these new methods. We focus on a single spacecraft repeat-pass InSAR mission and investigate the radar and mission parameters that would provide both high spatial resolution topography as well as the ability to detect subtle variations in the surface. Our preferred scenario is a longer-wavelength radar (S or L-band) placed in a near-circular orbit at 600 km altitude. Using longer wavelengths minimizes the required radar bandwidth and thus the amount of data that will be transmitted back to earth; it relaxes orbital control and knowledge requirements. During the first mapping cycle a global topography map would be assembled from interferograms taken from adjacent orbits. This approach is viable due to the slow rotation rate of Venus, causing the interferometric baseline between adjacent orbits to vary from only 11 km at the equator to zero at the inclination latitude. To overcome baseline decorrelation at lower latitudes, the center frequency of a repeated pass will be adjusted relative to the center frequency of its reference pass. During subsequent mapping cycles, small baseline SAR acquisitions will be used to search for surface decorrelation due to lava flows. While InSAR methods are used routinely on Earth, their application to Venus could be complicated by phase distortions caused by the thick Venus atmosphere.

© 2012 Elsevier Ltd. All rights reserved.

1. Motivation

Detection of present-day volcanic or tectonic activity on Venus would revolutionize our understanding of terrestrial planets (Crisp et al., 2002; VEXAG, 2007). The Earth and Venus have similar size, mass, and presumably similar composition. The Earth is highly active both tectonically and volcanically. If one were able to drain the oceans from the Earth, the volcanic and tectonic activity would be immediately obvious along all the mid-ocean ridges. Even on land, there are typically 20 active volcanoes at any one time. This activity is a primary heat loss mechanism for Earth. Assuming similar concentrations of radiogenic sources for Venus, the planet must also be volcanically active averaged over 1 billion-year timescales. There are two end-member possibilities (Solomon, 1993). First, Venus could be highly active volcanically and possibly tectonically, today. This would both release radiogenic heat as well as affect atmospheric chemistry just as hydrothermal vents replenish the ocean chemistry on the Earth.

The second possibility is that Venus was highly tectonically active (with associated widespread volcanism and perhaps lithospheric overturning) before ~500 Ma ago but then went into a period of inactivity that continues to this day (Turcotte, 1993). In this second model, the input of volcanic gases into the atmosphere in the recent past would have been more limited. Distinguishing between these two end member models would dramatically increase our understanding of Venus geodynamics, geology, and atmospheric science.

As the dense atmosphere of Venus prevents optical imaging of the surface, microwave remote sensing offers the best opportunity to search for present-day activity or at least identify the most recently active areas that could be explored by a surface lander mission. In the nearly 20 yr since the Magellan radar mapping of the surface of Venus, Earth radar imaging methods have evolved such that repeat-pass radar interferometry is now considered a routine method for measuring surface topography at high spatial and vertical resolution as well as for measuring surface change due to volcanoes, earthquakes, and other ground deformation (Massonnet and Feigl, 1998). The application of InSAR for mapping of planetary bodies including Venus has also been proposed (Ghail et al., 2012). The basic requirements for repeat-pass InSAR are: (1) the radar must be phase preserving and provide adequate

* Corresponding author at: Geophysical Institute, University of Alaska Fairbanks, 903 Koyukuk Drive, Fairbanks, AK 99775, USA. Tel.: +1 907 474 7767; fax: +1 907 474 7290.

E-mail address: fjmeyer@alaska.edu (F.J. Meyer).

sampling in the along-track and across-track coordinates (discussed below); (2) the surface being imaged cannot change significantly between the times of the reference and repeat acquisitions; (3) the reference and repeat orbits must be nearly parallel and the distance between the orbital paths must be less than a critical value which is a function of the radar characteristics (discussed below); and (4) finally the spatial variations in the atmospheric phase delay must be small enough to recover phase differences due to topography or surface change. This last criterion is particularly relevant for Venus and it is the major uncertainty in estimating the scientific utility of a repeat-pass InSAR mission on Venus.

The topography of the Earth has been measured using three types of InSAR configurations. The fixed baseline configuration of the SRTM mission (Farr et al., 2007) provided the first global mapping of the Earth's topography at 30 m pixel size and 5–10 m vertical accuracy. Since the reference and repeat phase maps are collected (almost) simultaneously across the fixed 60-m baseline, atmospheric phase distortions cancel out during the formation of an interferogram. Currently the German Aerospace Center (DLR) is operating TanDEM-X, an InSAR mission where two satellites fly in close formation, to map the topography of the Earth at 5 m resolution and decimeter-scale vertical accuracy (Krieger et al., 2007). The two spacecraft fly in a so-called helix formation at a spatial separation of about 350 m. Their maximal along-track separation is always less than 46 ms, causing atmospheric distortions to nearly cancel out between the two measurements. The across-track baseline can be adjusted for optimal topographic sensitivity over various surfaces (Gonzalez et al., 2010; Krieger et al., 2007). The third configuration is the standard repeat-cycle interferometry mode (Zebker and Goldstein, 1986) where the reference and repeat images are acquired on successive orbital cycles of perhaps 35 days (e.g., ERS-1/2, Envisat). The advantage of this approach is that only one spacecraft is needed and interferometric baseline can be adjusted to optimize the vertical sensitivity of the topographic map (discussed below). Of course phase differences due to changes in the atmosphere over the 35-day period may introduce significant distortions that map directly into the topographic model (Gong et al., 2010; Hanssen, 2001; Meyer et al., 2008). One novel approach to topographic mapping was demonstrated by the European Space Agency by flying the ERS-2 and Envisat satellites in a tandem configuration (Wegmüller et al., 2009; Wegmüller et al., 2009). The almost simultaneous acquisition of SAR images by these satellites allows for the generation of a new type of interferogram characterized by a short 28 min repeat-pass interval. However, because of their slightly different center frequencies, interferograms formed between acquisitions of these satellites show coherence only under particular conditions (discussed below). Only for a baseline of about 2 km can the spectral shift caused by differences in incidence angles (discussed below) compensate for the carrier frequency difference. Given the large spatial baseline and the short time lag between acquisitions, ERS-ENVISAT interferometry has the potential to generate precise digital elevation models (DEMs) in relatively flat areas. In the example in Fig. 1, acquired with a baseline of about 2.1 km, topography was mapped with a precision of about 50 cm. The InSAR concept proposed in this paper is based on the experience gained from the ERS-ENVISAT interferometry experiments.

Detecting and measuring surface change on the earth is now routinely performed using repeat-pass InSAR. The applications include: monitoring all three phases of the earthquake cycle (co-, post-, and inter-seismic deformation) along major faults (Chlieh et al., 2004; Ryder et al., 2007; Wei et al., 2010; Wright et al., 2003); measuring vector velocities of ice streams in Greenland and Antarctica (Kenji and Kaufmann, 2003; Meyer, 2007; Rignot et al., 2001, 2002, 2008; Strozzi et al., 2008) and monitoring surface deformation

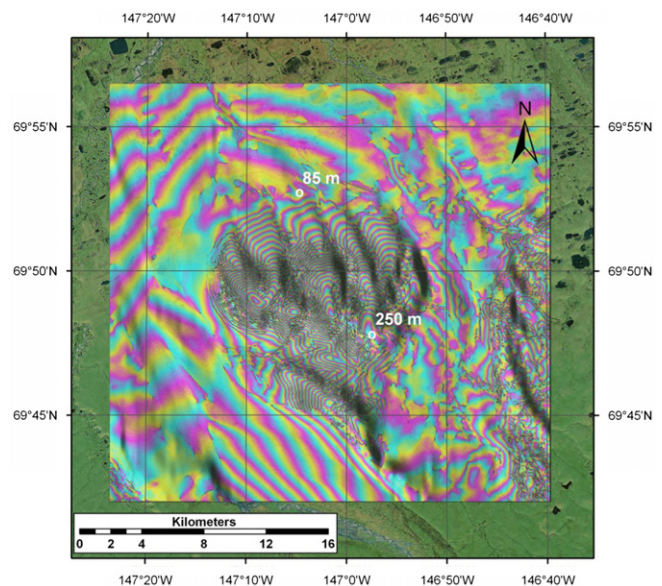


Fig. 1. ERS-2/ENVISAT ASAR cross-platform interferogram. The time delay between the acquisitions was about 30 min. The interferometric baseline corresponds to $B_{\perp} = 2150$ m so one fringe represents 3.8 m of elevation change. The ERS-2/ENVISAT ASAR constellation can serve as a proxy for pass-to-pass InSAR acquisitions on Venus.

due to natural and human-induced motions of crustal fluids (e.g., water, oil, and CO_2) (Ferretti et al., 2000, 2001; Fielding et al., 1998; Hoffmann et al., 2001; Meyer et al., 2007; Stramondo et al., 2008; Teatini et al., 2012). The technique is now mature and satellite systems are being developed where repeat-pass InSAR is their primary objective (e.g., ALOS-2 (Suzuki et al., 2009)). Temporal decorrelation is the major limitation for performing InSAR on the Earth. This decorrelation usually occurs because the radar scatterers within each pixel change due to changes in vegetation structure, rain, or snow. The longer wavelength radar systems provide longer decorrelation times to enable deformation mapping in moderately vegetated areas. In desert areas with low rainfall, it is possible to retain interferometric coherence for more than 10 yr. Since Venus lacks vegetation and water, we expect high correlation over very long timescales unless the surface is disturbed.

For change detection on Venus there are three possible approaches using SAR and InSAR methods: changes in radar backscatter; temporal decorrelation, and InSAR phase changes.

Backscatter—The most straightforward way in which new surface volcanic activity might be detected is mapping differences in radar backscatter from one observation to the next. Such a difference might be produced either by the eruption of a radar-bright (rough, possibly a'a) lava flow on top of a radar-smooth (pahoehoe-like) lava flow, or the inverse process wherein radar dark flows emplaced on top of radar bright units. Such changes were detected using ERS-1 radar images of Westdahl and Mt. Spurr volcanoes in Alaska (Rowland et al., 1994), which erupted between successive observations by the ERS-1 radar system. A candidate location for recognizing this type of activity on Venus might be Sif Mons where there are extensive radar-dark materials at the summit immediately to the west of the caldera.

Correlation—Repeat-pass interferometry can be used to detect surface change by examining the correlation between the reference and repeat images. This approach only requires that there is spectral overlap (discussed below) between the reference and repeat images. The method does not require an accurate digital elevation model for correction of the topographic contribution to phase, so only two passes are needed to detect surface change. There are three candidate processes for surface disturbance on Venus. The first is

sedimentation of fine particles such as the debris that forms the halos around impact craters (Greeley et al., 1992). To reduce the interferometric correlation the thickness of the deposits should be greater than $1/2$ the wavelength of the radar (e.g., 2 cm for C-band and 12 cm for L-band). The second process causing surface decorrelation is the occurrence of a lava flow between the times of the reference and repeat orbits. Correlation analysis is an established technique for mapping lava flows on Earth (Poland et al., 2008; Zebker et al., 1996). Changes in the lava flow may not be apparent in the radar backscatter images but any small changes in the surface scatters either due to superposition of a new flow or inflation of an existing flow will cause nearly complete surface decorrelation. As shown in Fig. 2 this approach of decorrelation mapping is the standard operating method used by the USGS to monitor flow

activity at the Kilauea, Hawaii volcano (M. Poland, personal communication, 2009). The third process that could cause decorrelation is landslide activity in steep mountainous areas. However landslides necessarily occur in steep areas where the interferograms could have slope decorrelation if the baseline of the reference and repeat passes is too large. While it is possible to use decorrelation maps to detect surface change in steep areas, the approach is more suitable for the relatively flat (slopes $< 10^\circ$) lava fields.

Phase—The phase of an interferogram can be used to detect surface topography as well as very subtle surface displacements having line-of-sight motions greater than $\sim 1/10$ of the radar wavelength (~ 2 cm in L-band and ~ 0.5 cm in C-band) (Zebker et al., 1994). InSAR is an established approach for monitoring volcano inflation/deflation on the Earth (Fig. 3). The requirements for

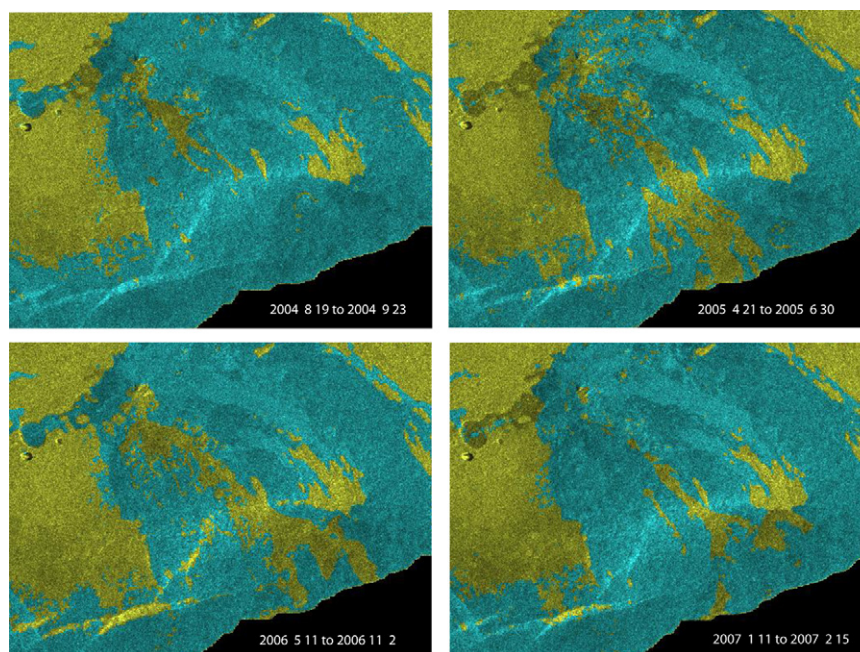


Fig. 2. Maps of decorrelation due to lava flows at the East Rift zone of Hawaii derived from Envisat (C-band) radar interferometry. This is the standard approach used by the USGS to map the flow sequences (M. Poland, personal communication, 2009).

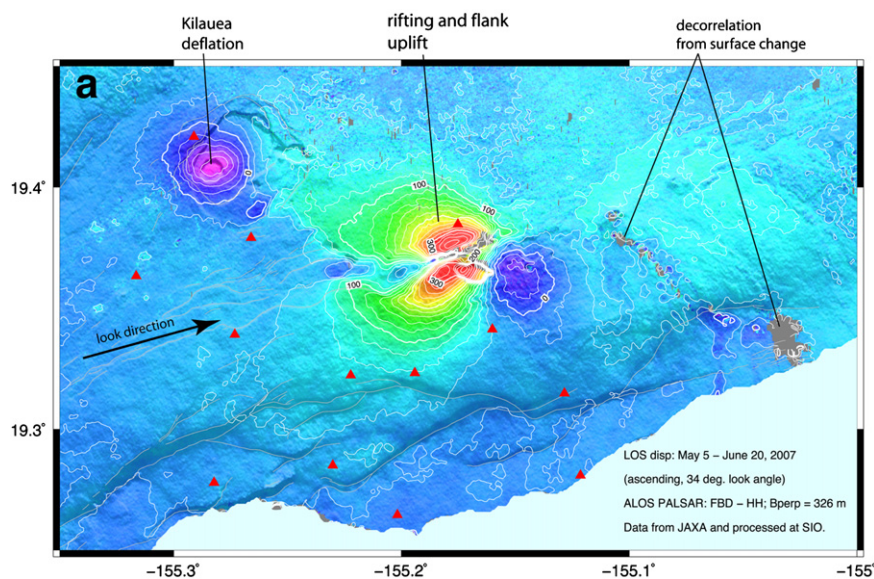


Fig. 3. Displacement map (contour interval 20 mm) of Kilauea volcano, Hawaii, showing deflation over the summit caldera (presumably due to magma withdrawal from the shallow reservoir) and inflation due to dike injection along the East Rift Zone. These data are derived from ALOS interferometry at a wavelength of 24 cm (Sandwell et al., 2007). Displacements as small as 5 mm can be mapped using this approach.

constructing accurate phase maps are much more stringent than requirements for constructing correlation maps. A high-resolution digital elevation model is needed to remove the topographic phase contribution and isolate the deformation signal. On Venus, this requires a three-pass approach where two short timespan images are used to construct the DEM and a third long timespan image is used to detect the change. The advantage of this approach is that in addition to volcano deformation due to, say, the inflation or deflation of a shallow magma chamber, or to the intrusion of a new dike close to the surface, any possible changes associated with a shallow and large Venus quake (> magnitude 6) could be mapped. Detecting quake deformation of Venus is very unlikely as no a-priori information on the location of these quakes is available. Also, these types of large events are probably rarer on Venus than on the tectonically active Earth. Nevertheless, mapping of shallow quake deformation associated with a highly active volcano is possible. Note that because of the high surface temperature on Venus, it is unlikely that a quake on Venus would generate elastic waves because the material would most likely be velocity strengthening (Dieterich, 1994).

While InSAR has become a routine way to monitor small surface changes on Earth, there are several environmental and technical challenges that could prevent a similar program on Venus. The major unknown is the amplitude and spatial signature of atmospheric phase distortions on the radar signal. A well-stratified atmosphere on Venus may only produce long-wavelength phase distortions that could be corrected using the large-scale altimetry DEM available from Magellan. Atmospheric phase effects on a scale less than the swath width of the radar could produce effects ranging from mild phase distortions to complete decorrelation of the interferograms. While total phase distortions would be a showstopper for any InSAR mission and would also create severe distortions in SAR amplitude images, InSAR measurements from ground-based radio telescopes have resulted in coherent interferograms of Maxwell Montes on Venus (see Fig. 4) (Carter et al., 2006). A personal communication from Jean-Luc Margot notes the following “We know that coherence is

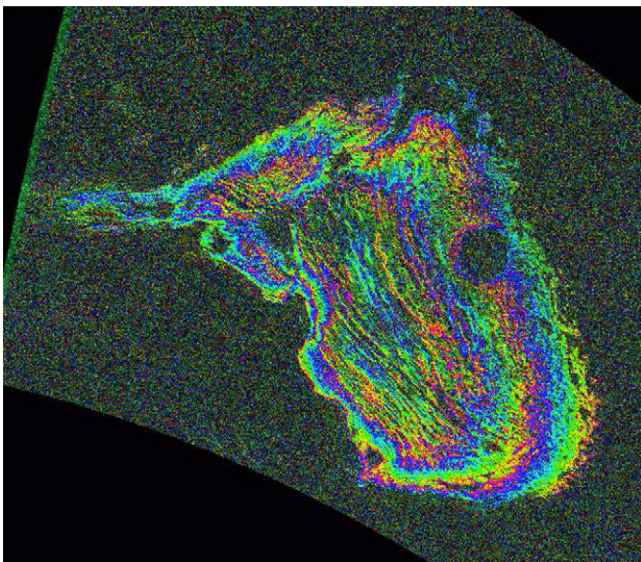


Fig. 4. Radar interferogram of Maxwell Montes derived from Arecibo Observatory and Green Bank Telescopes to obtain interferometric observations of Venus (Carter et al., 2006). The Arecibo radar was used to transmit a circularly polarized 12.6 cm wave, and the echo was received at both telescopes. The resulting maps have a spatial resolution of 1–2 km, and the height resolution of the topography is about 200 m. Data were acquired in 2001 and 2004; changes in viewing geometry and improvements to the Arecibo telescope increased the signal to noise for the later observations.

preserved for at least ~ 300 s at S-band based on our imaging. I also have a handful of X-band data points that show coherence being maintained over time periods from 20 s to 150 s. Moreover, the strength of the correlation does not appear to depend on the time interval.” These results and the message have two important pieces of information. First the imaging time was 300 s. As discussed below, we need to maintain coherence over 6000 s for pass-to-pass interferometry and 243 days for repeat-pass interferometry. The pass-to-pass requirement is only 20 times longer than what has been demonstrated. The second key piece of information is that InSAR works at X-band for 20–150 s. The atmospheric phase distortions at X-band will be 8 times worse than at, e.g., S-band. This suggests that atmospheric distortions may not significantly reduce phase coherence for pass-to-pass interferometry. In addition a recent study by Hensley and Shaffer (2010) shows a single 243-day interferogram from Magellan SAR data suggesting repeat-pass InSAR is possible. Nevertheless, atmospheric variations remain an uncertainty in InSAR processing. We will show that the InSAR concepts presented in this paper are effective in reducing the impact of atmospheric phase delay on InSAR coherence and phase analysis.

With this paper we propose several SAR interferometry concepts for a single-antenna mission to Planet Venus. Detailed descriptions of the concepts are provided and accompanied with an analysis of performance as well as pros and cons compared to other more traditional InSAR methods. All analyses are based on a hypothetical mission design that follows a Magellan-like orbit configuration. C-band, S-band, and L-band configurations are analyzed and compared for their relative performance. Based on the analyses in this paper, a recommendation for an optimal mission design is provided.

In Section 2, the conditions of InSAR on Venus are analyzed. Two different InSAR concepts, specifically adapted to the characteristics of Venus are introduced in Sections 2.4 and 2.5. A discussion on atmospheric phase distortions on InSAR at Venus is presented in Section 2.6. Section 3 summarizes how InSAR observations can contribute to a better understanding of the history and evolution of planet Venus. The paper ends with conclusions and recommendations for preferred system configurations (see Section 4).

2. InSAR concepts for the planet Venus

SAR Interferometry (InSAR) on Venus faces a different set of challenges than similar endeavors on Earth. Besides the influence of the dynamic and very dense atmosphere on amplitude and phase of radar signals, it is the shape and slow rotation of the planet that define challenges and opportunities of InSAR at Venus. In the following sections two different InSAR concepts are introduced and compared with respect to their relative performance and their applicability to Venus. An introduction to the principles of InSAR can be found in Appendix A1.

2.1. A hypothetical SAR instrument

The following analysis of general InSAR concepts is based on a hypothetical SAR system, whose main orbit parameters and acquisition geometries are based upon the characteristics of the Magellan mission, which successfully orbited and mapped Venus from 1990 to 1994. One key parameter to be selected carefully for a mission to Venus is the center frequency of the system. Shorter wavelengths are more sensitive to distortions of the turbulent Venus atmosphere and impose stronger restrictions on InSAR baseline selection (see Section 2.5) yet may allow for improved image resolution. Longer wavelengths, while being advantageous

for InSAR baseline planning and showing less sensitivity to the neutral atmosphere, may be affected by ionospheric distortions on the dayside of the Venus. To provide a general study of potential InSAR configurations, three frequency bands, C-band, S-band, and L-band are analyzed. The basic system parameters are summarized in Table 1. A summary of the orbit geometry considered in this paper is given in Section 2.2.

Table 1 provides likely numbers for the maximum signal bandwidth W_{\max} that are realistically implementable for a Venus-observing SAR system in C-, S-, and L-band. In most situations, the real signal bandwidth W will be less than W_{\max} due to data rate limitations. In addition to system parameters, also values for the *critical baseline* $B_{\perp,crit}$ are included in Table 1. The critical baseline is the maximum baseline length for which interferometry is still possible and is an important parameter for the development of InSAR concepts. It is directly related to the other parameters listed in Table 1 (see Eq. (A-4) for more details), and amounts to $B_{\perp,crit,max}=9,17$, and 33 km for C-, S-, and L-band, respectively.

2.2. Orbit considerations

To facilitate a system capable of repeat-pass InSAR, the orbit of a satellite has to be designed such that it closely (within a distance smaller than $B_{\perp,crit}$) repeats a ground track from a previous cycle after a fixed period of time in both location and orientation. To accomplish this, knowledge of the physical characteristics of the orbited planet as well as information about nominal orbital parameters are required. The relevant parameters for Venus and Earth are provided in Table 2. While many of the parameters are similar for both planets, it is the small ellipticity of Venus (represented by the dynamic form factor J_2), as well as its

slow rotation that cause most of the differences in orbit behavior and progression.

In this analysis we consider a sensor flying in a circular orbit at a nominal altitude of $h=600$ km for both Venus and the Earth. The orbital period T_s for a system orbiting at radius $a=R_p+h$ about a planet of mass M and radius R_p is given by Kepler's third law

$$T_s = 2\pi \sqrt{\frac{a^3}{GM}} \quad (1)$$

where G is the gravitational constant. For both Venus and the Earth the orbital period is about 98 min at this altitude. An inclined orbital plane will precess with respect to an inertial frame at a rate that depends on the orbital radius a , the orbital inclination i , and the dynamic form factor J_2 .

$$\frac{w_n}{w_s} = \frac{-3R_p^2}{2a^2} J_2 \cos(i) \quad (2)$$

where $w_s=2\pi/T_s$ is the orbit frequency and w_n is the precession frequency of the node. Many earth orbiting satellites are placed in a sun synchronous orbit where the orbital plane precesses exactly once per year. As the J_2 of Venus is about 150 times smaller than that of the Earth, the orbital plane will remain essentially fixed in a Venus-centered non-rotating reference frame, and is also largely independent of orbit inclination i . Therefore, the inclination of the orbit can be selected based on scientific merit. As an example, the Magellan spacecraft had an inclination of 86° to completely map the surface of Venus. For this paper, we have selected the same inclination, as global surface mapping with high resolution is a likely goal of a future mission to Venus.

Besides the J_2 parameter, the major difference between Earth and Venus relevant to radar remote sensing is the slow rotation rate of Venus, which is completing one revolution every 243 Earth days. With this slow rate and the fixed orbital plane, the ground track of a satellite is almost a great circle path. Successive orbits have ground tracks that are offset by only 10.8 km at the equator, decreasing to zero at the maximum inclination of the satellite. If placed at 600 km altitude, a satellite system at Venus would therefore repeat a previous orbit after 3507 revolutions around the planet. This orbit configuration has three implications for mapping the surface with synthetic aperture radar:

- Adjacent tracks are spaced at less than ~ 11 km. Thus, to achieve complete coverage of the surface, the swath width of the radar should be greater than 11 km. Earth orbiting SAR's typically have a swath width of 70–100 km so every part of Venus can be imaged in one 243-day cycle using an Earth-capable radar. Moreover, if the swath width is reduced, this also reduces the total amount of data that needs to be transmitted back to Earth, which is advantageous as many interplanetary missions are data-rate limited.
- As discussed in Section A1.1 (see Appendix A), conventional *repeat-pass interferometry* for topography and change detection requires that the reference and repeat tracks be spaced no greater than about 1/4 the critical baseline $B_{\perp,crit}$. As shown in Table 1 and analyzed in more detail in Section 2.5.1, for most conventional SAR instruments, this spacing is significantly less than 11 km and conventional repeat-pass interferometry could only be applied after one repeat cycle of 243 days has been completed.
- While standard repeat-pass InSAR requires small track spacing, the relatively close spacing of adjacent orbits (< 11 km) may allow for the implementation of *pass-to-pass interferometry*, a modified InSAR concept that will be discussed in detail in Section 2.5

Table 1
System parameters and standard observation geometry.

Orbit height (circular orbit)	H	600 km
Range to object	ρ	750 km
Wavelength:	λ	
C-band		0.0566 m
S-band		0.1260 m
L-band		0.2460 m
Max. signal Bandwidth:	W_{\max}	
C-band		100 MHz
S-band		80 MHz
L-band		80 MHz
Critical Baseline:	$B_{\perp,crit}$	
C-band		Up to: 9 km
S-band		Up to: 17 km
L-band		Up to: 33 km
Look angle	θ	35 deg
Range of surface slopes	α	± 20 deg

Table 2
List of planetary and orbit parameters.

	Venus	Earth
Mass M	4.86×10^{24} kg	5.97×10^{24} kg
Average radius R_p	6052 km	6371 km
J_2	6.92×10^{-6}	1.082×10^{-3}
Rotation period	–243.02 days	1 days (86,400 s)
Orbit altitude	600 km	600 km
Orbit period T_s	5958 s	5787 s
Orbit inclination	86	98
Orbit precession rate	–	365 days
Track spacing at equator	10.8	2600 km

2.3. The Venus terrain as a prior for mission design

Due to the transfer rate limitation of the Deep Space Network, the amount of generated data per unit area has to be minimized in order to maximize the surface area that can be imaged in a given time. This can be accomplished by minimizing the required range bandwidth, which, according to Eq. (A-3), depends on the length of the interferometric baseline, the range of local surface slopes α , the wavelength of the system λ , and the range to the object on the ground ρ , and can be calculated if these system parameters as well as the range of expected surface slopes on Venus are known.

Substantial amount of information about the topography of Venus is available from the Magellan mission where topographic information was extracted from altimetry data (Ford and Pettengill, 1992) at 10–20 km resolution, as well as stereo-processed SAR imagery (Herrick et al., 2012) at 1–2 km resolution. Additional statistical analyses of surface slopes on Venus were published in Ford and Pettengill (1992) based on altimeter mode radar data of the Magellan mission (see Fig. 5).

This information can be used to optimize both the design and operation of an InSAR system around Venus in several ways. For instance, available low resolution topographic information can be applied to remove errors in InSAR-derived DEMs that are caused by the limited knowledge of the SAR sensor's orbit. In a least-squares optimization approach, orbit errors can be estimated and corrected by minimizing the difference between topographic information available from previous missions and a low pass filtered version of InSAR-derived DEMs. The incorporation of available topography information will therefore lead to more accurate InSAR-derived products and to a better understanding of orbital dynamics.

As will be shown in Sections 2.4 and 2.5, available topographic data can be utilized in a second way: Statistical information about the surface slope distribution can be incorporated in order to determine bandwidth requirements for an InSAR-based topographic mapping mission at Venus. As shown in Fig. 5, surface slopes of Venus are rather shallow. A statistical analysis shows an average surface slope of 2.84° ; 95% of the surface has surface slopes of 6° or less, and 99% of the surface has slopes of less than 9° . The upper bound on surface slope is about 20° . Two slope ranges are assumed in the analyses of optimized InSAR configurations presented in Sections 2.4 and 2.5. A slope range of $\alpha = \pm 6^\circ$ is used to define InSAR system parameters that allow successful mapping of 95% of Venus' surface. Additionally, a slope

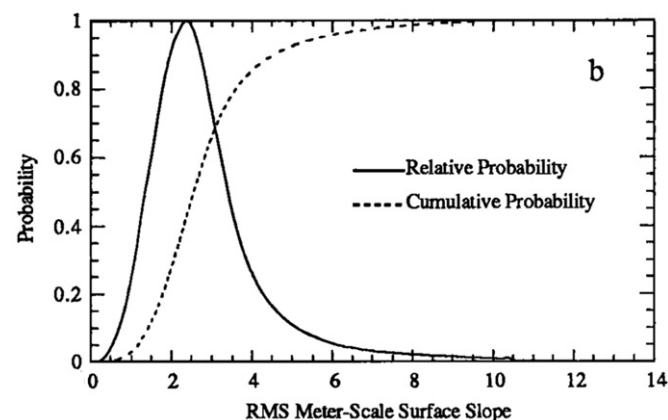


Fig. 5. Distribution of meter-scale surface slopes on Venus [deg]. The data was derived from altimeter mode radar data of the Magellan mission. Extracted from Ford and Pettengill (1992).

range of $\alpha = +20^\circ$ is analyzed to determine system parameters required for mapping the 5% surface area with high relief.

2.4. Repeat-pass InSAR on Venus

As explained in detail in the Appendix (see Sections A1.1.1 and A1.1.2), to achieve phase coherence in InSAR, the reference and repeat orbits used in interferogram formation must be nearly parallel, and the perpendicular separation of the orbit paths must be less than the critical baseline (see Eq. (A-4) in Section A1.1.1 for a definition of the critical baseline). For a repeat-pass constellation, it can be safely assumed that the orbits are sufficiently parallel to achieve good coherence. Here we investigate briefly the effects of non-zero perpendicular baseline on coherence to provide the mathematical basis for a comparison of repeat-pass InSAR with other InSAR concepts presented below. Repeat-pass interferometry satellites orbiting the Earth typically control the orbit such that the perpendicular baseline is less than +1000 m. Here we assume the same level of orbit control for a Venus mission, which is sufficiently below the critical baseline for all systems under consideration (cf. Table 1).

In (across-track) interferometry, two images observing the ground from slightly different across-track locations are combined to form an interferogram. Due to their difference in observation geometry, expressed by slightly different look angles θ , slightly different sections of the object spectrum are observed by the two acquisitions. The size of the relative spectral shift $\Delta f(\alpha)$ between the observed object spectra can be calculated by Eq. (A-3) and increases with the spatial baseline that separates the two acquisition locations. If this frequency shift is larger than the system's bandwidth W , the information in the interferometric partner images does not overlap anymore and the interferogram decorrelates. Knowing the frequency shift associated with InSAR constellations is therefore important to determine InSAR performance and sensor bandwidth requirements.

Fig. 6 shows the frequency shifts $\Delta f(\alpha)$ for a maximum repeat-pass baseline of $B_{\perp} = 1000$ m as a function of center frequency (C-, S-, and L-band) and local surface slope. The calculations are based on Eq. (A-3) and use the system and orbit parameters of Table 1 and Table 2. Fig. 6A shows relative frequency shifts for the range of surface slopes that are likely to occur on Venus (cf. Section 2.3 for details), while Fig. 6B shows $\Delta f(\alpha)$ for the entire range of possible α angles. Based on this calculation we conclude that the average frequency shift $\mu_{\Delta f}$ for slopes of $\alpha = \pm 20^\circ$ is relatively small (C-band 15.6 MHz, S-band 5.3 MHz, and L-band 2.7 MHz). From $\Delta f(\alpha)$ we can also derive the minimum radar bandwidth W_S that is required to achieve coherence across slopes a predefined range of surface slopes. For $\alpha = \pm 20^\circ$, W_S results in $W_S^{B=1\text{km}} = 52.7$ MHz, 23.7 MHz, and 12.1 MHz, for C-, S-, and L-band radars. To map the 95% of the planet's surface with slopes $< \pm 6^\circ$ the required bandwidth reduces to 25.6 MHz, 11.5 MHz, and 5.9 MHz for these three carrier frequencies. The parameter W_S also defines the amount of data per image frame that needs to be downlinked to Earth. It is therefore an important parameter in defining the amount of Venus surface that can be imaged per orbit cycle, given a predefined downlink data rate. Fig. 6B shows that, if the SAR system is operated using a minimal signal bandwidth W_S , all surfaces except slopes between 21° and 46° could be imaged (see area of blind angles). If the range of surface slopes for a given area is known, bandwidth requirements can be adaptively changed to minimize data volume while keeping InSAR performance.

In addition to the coherence consideration, it is important to evaluate the vertical precision with which surface topography can be mapped with the described C-, S-, and L-band radars. The relevant parameter is *phase-to-height sensitivity* $\partial\phi/\partial z$ which expresses the phase difference that is caused by a height

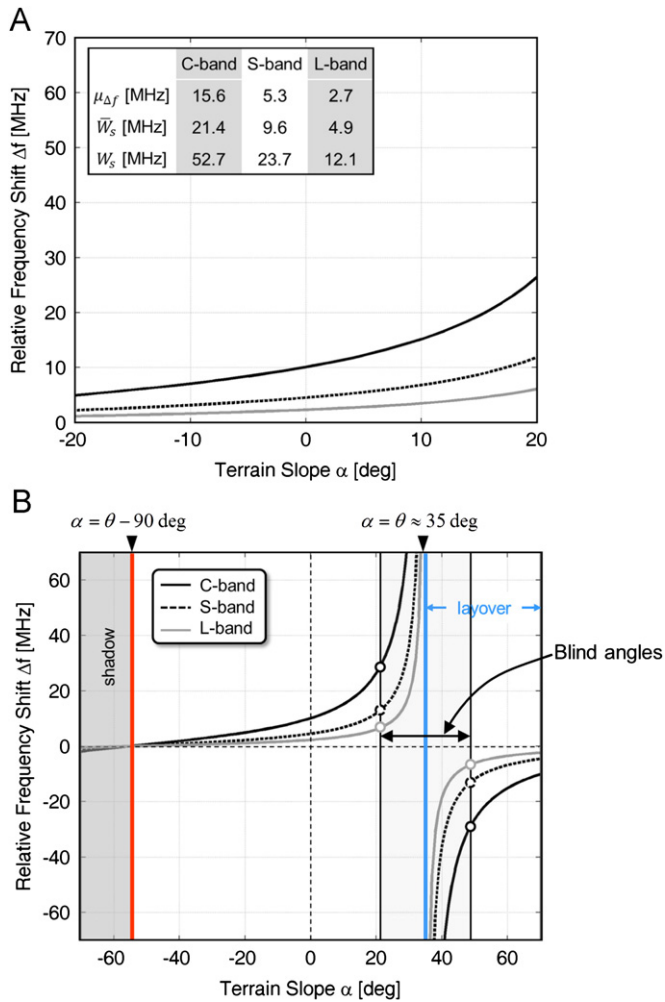


Fig. 6. Relative frequency shifts for an interferogram with $B_{\perp, \text{effective}} = 1$ km; (A) for terrain slopes of $\pm 20^\circ$; (B) for the entire range of possible α .

difference Δz between two resolution cells

$$\frac{\partial \phi}{\partial z} = \frac{4\pi}{\lambda} \frac{B_{\perp}}{R \sin(\theta)} \quad (3)$$

In Eq. (3), ϕ is the interferometric phase, z is topographic height, λ is the wavelength of the system, θ is the sensor's look angle, and R is the range between sensor and imaged surface. For the system parameters in Table 1 and considering an interferometric baseline of length $B_{\perp} = 1000$ m as well as $\theta = 35^\circ$, the ambiguity height $\Delta z_{2\pi}$ (the height difference that causes a phase shift of 2π) corresponds to $\Delta z_{2\pi} = 12.2$ m, 27.1 m, and 52.9 m for C-, S-, and L-band, respectively. This number can be used to determine fringe density and phase unwrapping challenges for different terrain types on Venus.

From Eq. (3), the standard deviation of a height estimates \hat{z} under consideration of a given phase noise σ_{ϕ} can be derived

$$\sigma_z = \frac{\sigma_{\phi}}{\partial \phi / \partial z} \quad (4)$$

Given the parameters in Tables 1 and 2, and assuming $B_{\perp} = 1000$ m, $\theta = 35^\circ$, and $\sigma_z \approx 40^\circ$ (a typical value for average interferometric coherence and a moderate number of looks (Just and Bamler, 1994)), the topographic height of a point on the ground can be estimated with a standard deviation of $\sigma_z \approx 1.4$ m, 3.1 m, 5.9 m for the C-, S-, and L-band systems, respectively. Note,

that in a real application to Venus, the actual relative height accuracy will be lowered by atmospheric phase distortions, phase unwrapping errors, and orbital baseline uncertainties. Absolute height information (e.g., from Magellan altimetry) will be needed at discrete locations to construct a global topography model from relative height measurements.

2.5. Pass-to-pass InSAR concepts

While it is theoretically possible to recover topography using the repeat-pass configuration, there are a number of factors that may make the repeat-pass concept challenging and error prone. The long time delay between repeat observations (243 days) will increase the chance for temporal decorrelation to occur. More importantly, the long time delays also increase the chance for strong atmospheric artifacts from both the dynamic upper and the slower rotating but dense lower atmosphere to emerge in the data. The long time delays also limit the number of repeat acquisitions to a maximum of 7 for a typical 5-yr mission. Long time delay combined with only few repeats will complicate the separation of phase changes due to true ground deformation and surface topography.

The time delay can be reduced to about 6000 s by designing a coherent InSAR concept from adjacent orbits, called *pass-to-pass InSAR*. A viable pass-to-pass InSAR concept has a number of important advantages: (1) it would increase the quality of InSAR observations by minimizing atmospheric phase distortions while maximizing coherence; (2) due to an increase of observations for a particular target area the variance of estimated topography and deformation parameters can be reduced; (3) due to the long spatial baselines (see below), the ratio of the topographic phase signal to other, undesired phase components (e.g., noise, atmospheric artifacts) is increased, resulting in higher quality topographic height estimates; (4) an operational scenario where interferograms are created from adjacent as well as repeated orbits, will lead to a diversification of temporal baselines, improving the separability of topography- and deformation-related phase components; (5) observations at a range of temporal scales allows studying deformation regimes of different temporal dynamics. A pass-to-pass InSAR concept will also allow to demonstrate interferometry at an earlier stage of the mission (theoretically after the completion of the second orbit rather than after completion of the first cycle), providing important information for execution of the remainder of the mission.

Achieving coherence in a pass-to-pass configuration requires significant overlap between the observed spectra in both azimuth and range. Here we investigate how the radar system must be modified to achieve this requirement.

Depending on the geographic location on Venus, the interferometric baseline of a pass-to-pass InSAR pair maybe larger than the critical baseline, causing the observed object spectra to diverge (see Section A1.1.1). This effect can be compensated by either increasing the system's range bandwidth until $W \geq \max(\Delta f(\alpha)) \quad \forall \alpha = [-20^\circ, +20^\circ]$, or by introducing a baseline-dependent shift of the system's center frequency (adaptive frequency shifting) for the second acquisition of an interferometric pair. As the allowable bandwidth of an interplanetary mission is limited, adaptive frequency shifting is the preferred option.

The orbit tracks of adjacent orbits are not perfectly parallel, but converge towards the point of maximum inclination. Therefore, acquisitions from adjacent orbits will observe the same point on ground with different geometries, leading to a relative shift Δf_{DC} of the respective Doppler spectra. Depending on the size of Δf_{DC} relative to the system's azimuth bandwidth W_{az} , active Doppler steering may be required to preserve phase coherence.

2.5.1. Compensation of spectral shifts due to long spatial baselines

Range frequency shifts $\Delta f(\alpha)$ are analyzed for a pass-to-pass InSAR configuration with an effective baseline of $B_{\perp, \text{effective}} = 9$ km. This configuration resembles an InSAR pair acquired at low latitudes, close to the Venus equator. The spectral shifts are calculated from Eq. (A-3) for terrain slopes between $\pm 20^\circ$ and using the sensor and orbit parameters as summarized in Table 1 and Table 2. In addition to $\Delta f(\alpha)$, also the average spectral shift $\mu_{\Delta f}$, the signal bandwidth required if no frequency tuning is applied W_s , and the signal bandwidth required if adaptive frequency tuning is performed \bar{W}_s are calculated and used for further analysis.

For $B_{\perp, \text{effective}} = 9$ km, relative frequency shifts for C-, S-, and L-band systems are summarized in Fig. 7A and B for $\alpha = \pm 20^\circ$ and the entire range of surface slopes, respectively. The average frequency shift reaches $\mu_{\Delta f}^{B=9\text{km}} = 141$ MHz, 47.6 MHz, and 24.4 MHz for C-, S-, and L-band systems. To image all relevant surface slopes in a nominal SAR mode, a system bandwidth of

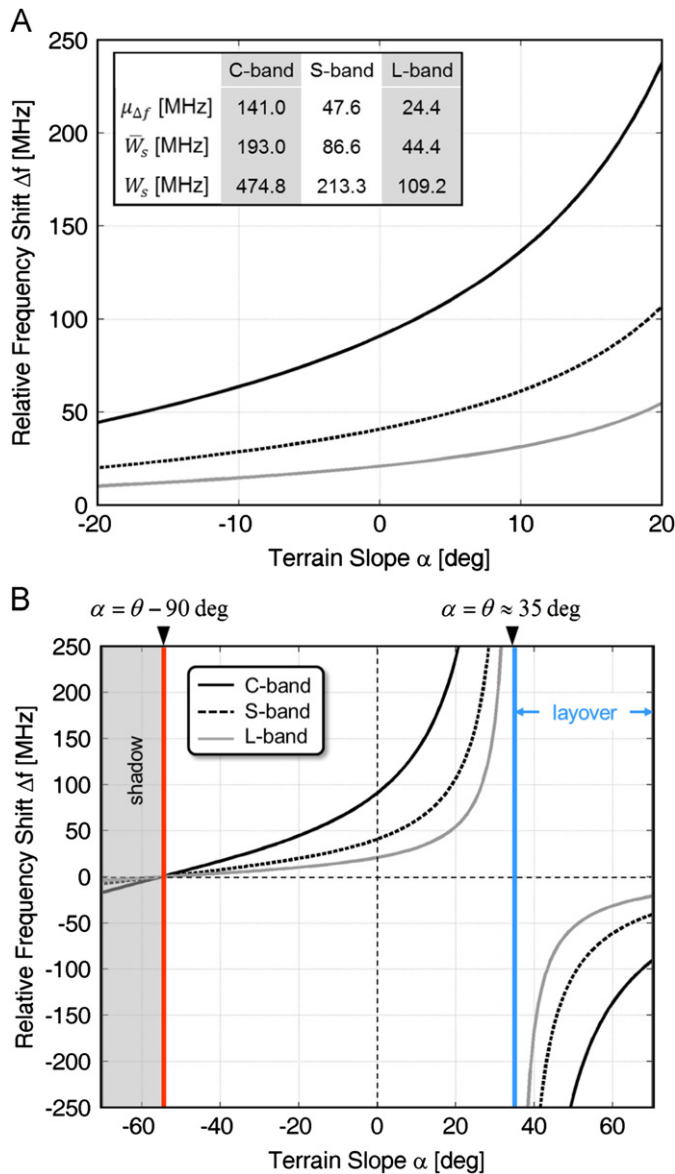


Fig. 7. Relative frequency shifts for an interferogram with $B_{\perp, \text{effective}} = 9$ km; (A) for terrain slopes of $\pm 20^\circ$; (B) for the entire range of possible α . Results for $\mu_{\Delta f}^{B=9\text{km}}$, $W_s^{B=9\text{km}}$, and $\bar{W}_s^{B=9\text{km}}$ are included in panel A. Calculations are based on the parameters in Table 1 and Table 2.

$W_s^{B=9\text{km}} = 475$ MHz, 213 MHz, or 109 MHz would be necessary (see Fig. 7A) for the different system center frequencies, each of which exceeding the bandwidth of conventionally available systems operating at the given center frequencies (cf. Table 1).

To overcome this problem, an adaptive frequency tuning of the transmitted signal is proposed to facilitate InSAR processing from adjacent tracks. Tunable interferometric satellite systems were first proposed in Gatelli et al. (1994). Based on available sensor, orbit, and baseline parameters, $\mu_{\Delta f}^{B=9\text{km}}$ can be derived and the center frequency of the sensor can be changed accordingly to compensate for the bulk of geometry-induced frequency shifts. After shift compensation, interferometric coherence can be achieved. Furthermore, the bandwidth requirements for coherently mapping all relevant surface slopes are minimized. In the above described scenario and after compensation of $\mu_{\Delta f}^{B=9\text{km}}$ the bandwidth required to image slopes of $\alpha = \pm 20^\circ$ can be reduced to $\bar{W}_{S, \alpha = \pm 20}^{B=9\text{km}} = 193$ MHz, 86.6 MHz, or 44.4 MHz, for C-, S-, and L-band. For $\alpha = \pm 6^\circ$, the required bandwidth shrinks to $\bar{W}_{S, \alpha = \pm 6}^{B=9\text{km}} = 41.5$ MHz, 18.7 MHz, or 10.0 MHz. If the topography of the area of interest is known and smooth, the required bandwidth can be even further reduced. Adaptive frequency shifting could therefore enable topographic mapping of large areas of the planet under realistic downlink capability. Please note that the bandwidth requirements $\bar{W}_{S, \alpha = \pm 6}^{B=9\text{km}}$ are calculated under the assumption that no volume decorrelation occurs. For operational processing, the available system bandwidth should be higher than $\bar{W}_{S, \alpha = \pm 6}^{B=9\text{km}}$, to accommodate potential volume decorrelation, sufficient spectral overlap at steep slopes, as well as uncertainties in the presumed surface slope range.

2.5.2. Compensation of Doppler shifts due to non-parallel orbits

When a common target on ground is imaged from adjacent orbits, the resulting SAR signals will have a different Doppler centroid if the antenna is oriented broadside to the orbital trackline. The overlap of the Doppler spectra of images from adjacent orbits can be increased by squinting one of the two passes using electronic beam steering, but the squint angle must be within the tolerance of the radar. A detailed discussion of Doppler centroid shifts caused by squinted orbit geometries can be found in Section A1.1.2.

The following assumptions are made for assessing required squinting maneuvers in a pass-to-pass configuration: (1) To reduce the mathematical complexity, the orbital inclination is increased from 86° to 90° ; (2) Doppler shifts introduced by the rotation of Venus are ignored by assuming a start-stop approximation where Venus does not rotate during acquisition of an image.

Under these simplified assumptions, the perpendicular distance s_{\perp} between orbits as a function of geographic latitude θ_{geo} can be described by

$$s_{\perp} = \omega_V T_s a \cos(\theta_{\text{geo}}) \quad (5)$$

where $\omega_V = 2\pi / (243 \times 86,400)$ is the rotation rate of Venus. The perpendicular velocity is the time derivative of the perpendicular distance given by

$$v_{\perp} = \frac{\partial s_{\perp}}{\partial t} = \omega_V T_s a \sin(\theta_{\text{geo}}) \frac{\partial \theta}{\partial t} = \omega_V T_s a \sin(\theta_{\text{geo}}) \omega_s \quad (6)$$

Assuming a target at a horizontal look angle for an initial worst-case calculation, the Doppler shift for a given v_{\perp} can be expressed as

$$\Delta f_{DC}(v_{\perp}) = 2f_0 \frac{v_{\perp}}{c} = \frac{2v_{\perp}}{\lambda} \quad (7)$$

where f_0 is the carrier frequency and the factor of 2 accounts for the 2-way path of the radar.

Evaluating Eqs. (5)–(7) using the parameters in Table 1 we arrive at

$$s_{\perp} \approx 11[\text{km}] \cos(\theta), \quad v_{\perp} \approx 11.65[\text{m/s}] \sin(\theta),$$

$$\Delta f_{DC}(v_{\perp}) \approx \begin{cases} 412 [\text{Hz}] \sin(\theta) & \text{at C-band} \\ 185 [\text{Hz}] \sin(\theta) & \text{at S-band} \\ 95 [\text{Hz}] \sin(\theta) & \text{at L-band} \end{cases} \quad (8)$$

As expected, the maximum separation between passes of 11 km occurs at the equator but the separation is less than 1 km at 85° latitude. The Doppler shift from adjacent orbits is largest for C-band systems, zero at the equator, and has a maximum of 412 Hz near the Poles. Note that the Doppler shift will be reduced by the sine of the look angle for non-nadir looking systems. As the estimated Doppler shift is far below the pulse repetition frequency of any existing spaceborne radar, electronic beam steering of the radar will not be required even for maximum Doppler shifts.

2.6. Atmospheric phase distortions

A major issue for measuring topography and surface change using repeat-pass interferometry is phase delays caused by the thick atmosphere of Venus. SAR interferometry is inherently a relative measurement; hence, if the phase delay through the atmosphere is the same on the reference and repeat acquisitions, the interferometric phase will remain undistorted. Moreover if the atmosphere is perfectly radially stratified, but time varying, then the only possible distortion is a phase ramp across the image in the range direction. Atmospheric phase variations will be a significant problem when their spatial correlation lengths are comparable to, or smaller than, the phenomenon being observed (topography or deformation).

Whether or not a repeat-pass InSAR mission around Venus will yield significant new information will depend on the ratio of topographic or deformation signal to atmospheric noise at spatial scales less than about the size of an image frame (swath width ~15–20 km). Typical atmospheric noise spectra for the Earth have been developed by Hanssen (2001) and Emdarson et al. (2003). On Earth, the atmospheric delay signal in SAR interferograms is dominated by water vapor variations in the troposphere (0–10 km) while the higher altitude stably stratified atmosphere has little effect on InSAR. The spectrum of atmospheric distortions on Earth is red. Hence, it is increasingly more difficult to observe larger-scale deformation patterns than smaller-scale signatures. To understand the effects of the Venus atmosphere on InSAR, typical power spectra of phase delay for Venus' very dense atmosphere need to be determined for the two relevant time scales of 100 min (for the pass-to-pass topography measurements) and 243 days (for the surface deformation measurements). To the best knowledge of the authors, such power spectra do currently not exist from either models or observations for the spatial scales that are relevant for InSAR. Methods for the development of atmospheric power spectra are currently under investigation (e.g., Duan et al., 2010). If these methods succeed, information may become available in the near future that can be used for developing meaningful bounds on scale and magnitude of atmosphere-related distortions.

Until such observations are available, the following considerations can help in bracketing atmospheric artifacts: The surface pressure of the Venus atmosphere is 92 times greater than the surface pressure of the Earth's atmosphere so if the Venus atmosphere has similar overall dynamics as the Earth, one would expect the phase distortions to be nearly 100 times worse. Fortunately, the atmosphere of Venus can be roughly divided into a stably stratified lower atmosphere having a radiative

cooling time scale of 100 yr (Crisp and Titov, 1997; Gierasch and Yung, 2002) and a more dynamic atmosphere above 50 km altitude. While the lowermost atmosphere (0–7 km) is adiabatically unstable, it is believed that pole-to-equator temperature variations, as well as wind speeds, are very low (< 1 m/s) in this region. Based on these observations and models (e.g., Duan et al., 2010), one would not expect significant changes in integrated vertical structure of the lower atmosphere (0–50 km), especially over the shorter 100-min timescale.

In contrast, the upper atmosphere of Venus is very dynamic and may change significantly over the previously mentioned relevant timescales. At 50 km altitude, the atmospheric pressure on Venus is similar to the surface pressure on the Earth. The region between 48 km and 64 km contains clouds with obvious retrograde zonal flow. In addition this region has a latitudinal temperature gradient, cooler toward the poles by about 20 K (Gierasch and Yung, 2002), that drives strong zonal winds. Winds in the uppermost cloud deck are about 100 m/s at lower latitude (< 50°) and quickly decrease in velocity with increasing latitude eventually reaching zero at the poles. The winds also have a strong vertical gradient that causes turbulent mixing and generation of gravity waves. Images from the Venus Express orbiter (Markiewicz et al., 2007) reveal that most of the gravity wave signatures have length scales greater than 50 km although smaller-scale waves (20–50 km) have been imaged at higher latitudes. The characteristic timescale of these features is about 1 day, which will mitigate their effects on the 100-min interval pass-to-pass InSAR measurements. However, upper atmosphere turbulence will most likely cause significant small scale (< 11 km) phase distortions in the 243-day interferograms used for change detection. Therefore we believe that the search for volcanic and tectonic deformations within the lifetime of a mission will be primarily based on the measurement of decorrelation rather than the observation of phase change.

The influence of atmospheric phase distortions on InSAR-based topographic height estimates is reduced by the temporal and spatial baselines configuration of pass-to-pass InSAR pairs (see Section 2.5 for details). Additional ways for reducing atmospheric influence is offered by existing information of the topography of Venus. The Magellan radar altimetry mission has provided topography on about an 11 km spacing. This information can be used to compensate large scale topographic phase contributions during interferogram formation. In the residual phase, only signatures smaller than 11 km are used for topographic mapping and only atmospheric noise with correlation lengths below this 11 km scale will lead to distortions in the topography estimates. This approach can significantly reduce the detrimental impact of the atmosphere on InSAR-based topographic mapping. Furthermore, as residual phase patterns with spatial scales above 11 km can be attributed to atmospheric delay, InSAR can also be used to study atmospheric turbulence patterns of spatial scales larger than 11 km.

2.7. An example scenario for the operation of a repeat-pass InSAR system at Venus

In this section, an example operation scenario of an InSAR mission at Venus is presented that benefits from the InSAR concepts that were presented above. With this study, we want to highlight that these InSAR concepts can allow for near-global topographic mapping as well as near-global coherent change detection with a mission that utilizes only one sensor and is operated for only a few Venus days.

An L-band system is assumed for this study, as the L-band wavelength reduces atmospheric phase distortions and lowers the required satellite-to-earth data transfer rates. It is furthermore assumed that this L-band SAR system is in a nearly circular orbit

at 600 km altitude, resulting in an orbital period of 6000 s (see Fig. 8). Please note that the choice of carrier frequency is uncritical from a technological point of view, as the InSAR concepts developed in this paper are viable at all studied frequencies.

For the following operation scenario, we assume that the mission goals include near-global high-resolution topographic mapping as well as a global analysis of surface changes that may indicate volcanic activity. The mission would furthermore focus on the areas of Venus with slopes less than 6° , which includes 95% of the surface of the planet. The swath width of the radar would be 22 km and the pulse repetition frequency would be ~ 2000 Hz corresponding to a single look along-track resolution of 2.6 m and an antenna length of 6 m.

Operations during the first Venus day would focus on *topographic mapping*. For this application, the SAR would operate in two modes. During even numbered orbits, the SAR operates at an L-band radar frequency of 1.22 GHz a bandwidth of 15 MHz and a nominal look angle of 34° . The 15 MHz bandwidth will provide coherent mapping conditions for all expected spatial baselines and all surface slopes within $\pm 6^\circ$. During the odd orbits, the look angle would be reduced by 0.5° so that the swath imaged on this odd orbit would fully overlap with the swath imaged on the previous even orbit. Using the same bandwidth, the center frequency would be adjusted according to Eq. (A-3) in order to compensate for the baseline dependent average frequency shift $\mu_{\Delta f}^B$ and to maximize the spectral overlap. $\mu_{\Delta f}^B$ will be calculated according to the local baseline conditions. At 15 MHz, a 22 km swath, and assuming a pulse repetition frequency of 2000 Hz, the data are collected at about 12 Mbits per second. If the time average downlink rate available through the Deep Space Network is less than this value, the even/odd imaging could be performed in latitude bands. Therefore, completion of global topographic mapping of Venus will depend on the available downlink resources and may take two or more cycles under unfavorable conditions. The pass-to-pass InSAR concepts would be applied for the generation of interferograms with high sensitivity to topography. The long spatial and short temporal baselines of the pass-to-pass InSAR data would also increase the ratio of topography to atmosphere-related phase signals and mitigate atmospheric distortions on the calculated topography. To further

reduce atmospheric influence, InSAR would be augmented with radargrammetry observations, where radargrammetry provides a good topography prior at low resolution in support of atmospheric phase filtering.

The *coherent change detection* objective of the mission will begin after one complete 243-day mapping cycle. Repeat orbits are adjusted to follow their reference orbit within a perpendicular baseline of less than 1000 m. These baseline restrictions are used to minimize topographic phase components and optimize the potential detection of deformation. Significant atmospheric phase distortions are expected in the repeat-pass interferograms. If the atmospheric fringe rate is lower than the range resolution of the radar (~ 30 m), intererometric coherence will largely be preserved, and can be used in coherent change detection efforts. For example, interferograms can be analyzed for areas of abrupt coherence loss associated with lava or debris flows. From analysis of phase signals, it may also be possible to detect potential, if unlikely, volcanic inflation events, if the produced deformation fringes dominate the atmospheric signal or differ from it in general spatio-temporal pattern. As the likelihood of a volcanic event during mission time is low, the focus of the change detection experiment component of the mission will be put on the analysis of coherence.

Due to the sensitivity of the system to atmospheric (and potentially ionospheric) delay, and due to the variety of temporal baselines that are possible by combining repeat-pass and pass-to-pass InSAR concepts, the analysis and understanding of atmospheric (and ionospheric) turbulence processes may be added as a secondary mission goal. Based on the experiences from early mapping cycles, the basic operating scenario could be modified for maximum science return.

3. Potential contribution of InSAR to the understanding of Venus

3.1. Precision topographic mapping

The proposed topographic mapping of Venus by pass-to-pass InSAR would be highly complementary to the global topography of Venus provided by Magellan altimetry at 10 km horizontal resolution and 50–100 m vertical accuracy (Ford and Pettengill, 1992) as well as the more limited (20% of Venus) stereo derived topography having 1–2 km horizontal resolution and vertical precision of 10's of meters. At a 9 km spatial baseline and assuming moderate phase noise levels of $\sim 60^\circ$, topography can be measured with a vertical precision in the order of 1 m at all analyzed system frequencies (see Eq. (3)). The exact precision depends on the amount of atmospheric phase distortions and can be determined from early pass-to-pass InSAR pairs. Depending on the bandwidth and center frequency of the radar, a horizontal resolution of about 100 m can be expected, revealing surface structures that were inaccessible from previous data.

While Magellan SAR amplitude imagery has resolved surface features at its 100 m resolution, one cannot separate dielectric, roughness, and slope variations from the backscatter intensity. The analysis of fine scale surface topographic structures could lead to breakthroughs in constraining the nature and timing of processes and events that have produced the current surface of Venus. Important scientific issues that could be addressed are related to volcanic, tectonic, impact, and Aeolian processes.

Volcanic features dominate the surface of Venus at all scales. New high-resolution topographic measurements would reveal the shape of the small shield volcanoes and domes that are pervasive on the surface of Venus. Collapsed lava tubes are evident in many areas yet the depths and downhill orientations of these tubes are

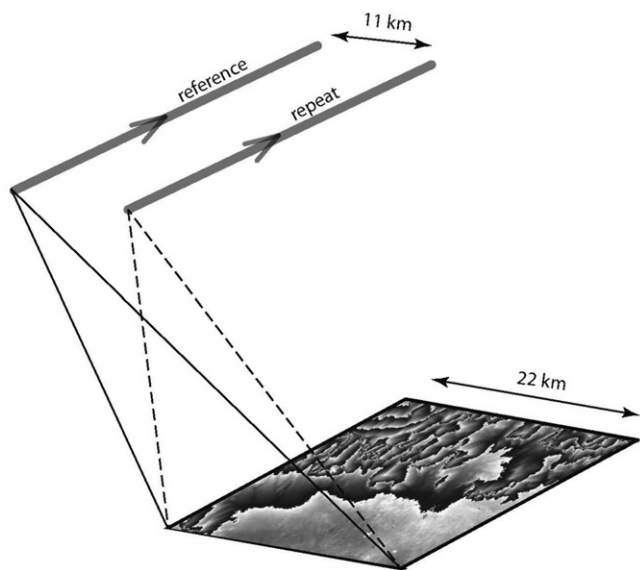


Fig. 8. Basic observation geometry of an L-band SAR system at Venus. The system's swath width is set to be 22 km. Adjacent orbits are separated by 11 km near the equator, leading to an interferometric baseline of about 11 km for a pass-to-pass interferogram.

poorly constrained (Roth and Wall, 1995). Large and small calderas cover the surface and many are surrounded by pits as well as radiating dikes. Measuring the third dimension of these features with high spatial and vertical resolution will be important for understanding their formation processes and associated surface strains. The importance of high-resolution topographic information was shown in previous studies where topography derived from Magellan radar altimetry revealed some notable surprises relative to the lower resolution Magellan altimetry data (Verner et al., 2011). At Anala and Kunapipi Mons, rifts through the volcano summit that were not resolved in altimetry were shown to be much deeper than they appeared in the images, significantly altering our views of the timing and lithospheric stresses involved in rifting and volcanism for those features. Similar achievements can be expected from InSAR-based high-resolution topographic mapping of features like Idunn Mons, which has received little geologic mapping attention despite its importance as a potential area for very recent volcanism (Smrekar et al., 2010). All existing data indicates that Idunn is a currently active Venusian hotspot over a mantle plume. High-resolution topography can help in the evaluation of the flow emplacement history at Idunn. It will also support studies of the evolution of the shape of the edifice as flow emplacement progressed, and will increase our understanding of the relationship of local rifting and fracturing to flow emplacement.

The surface of Venus is further covered with all types of fracture-like features whose origin has been attributed from rifting/diking to compression and wrinkle ridges. Measuring the vertical offset across these features will be important for constraining the magnitude of the horizontal strain during their formation (Bilotti and Suppe, 1999; Kreslavsky and Basilevsky, 1998). The detection and analysis of rift systems on Venus could also improve the understanding of the current thermal regime of Venus, how it has influenced surface geology, and how it has evolved over time (Grosfils and Head, 1996).

Impact craters of all sizes greater than a few kilometers are pervasive on the surface of Venus (Phillips et al., 1991). The stratigraphic history of impact craters can be used along with the volcanic stratigraphy to help unravel the tectonic history of the planet. Detailed topography measurements can provide important clues about the tectonic and volcanic modification of craters. Very high vertical resolution topography may reveal craters buried beneath thin lava flows. This would help to reveal the early resurfacing event that is the main evidence for a young average surface age of Venus.

3.2. Identifying change using coherent change detection methods

There is some limited evidence for current volcanic activity at Venus. The primary evidence comes from microwave emissivity and reflectivity of the planet as mapped by Magellan (Robinson and Wood, 1993). Most highland areas (greater than 3 km above the mean planetary radius) have low radiothermal emissivity (high reflectivity). It has been proposed that this results from weathering of rock at relatively lower temperatures (high elevation) producing high dielectric constant mineral assemblages (Klose et al., 1992). However there are a few volcanoes on Venus, with high elevation summits (as much as 8 km above datum for Maat Mons), where the highest elevations have high emissivity. It has been proposed that these anomalous areas are covered by relatively “young” lava flows where the weathering process has not had sufficient time to lower the emissivity. The timescale for the weathering process could be millions of years so these observations do not confirm activity today.

Secondary evidence for volcanoes being active today comes from stratigraphy and morphology of lava flows. For example on Maat Mons, lava flows of medium radar brightness overlie all

other landforms. Moreover there are volcanic domes on the summit of Maat Mons where most other volcanoes have calderas. Intra-caldera activity on Earth typically occurs on a timescale of a few tens of years for active basaltic shield volcanoes, so the presence of domes could indicate present-day activity.

Additional more speculative evidence for present-day volcanic activity comes from observations of temporal variations in atmospheric sulfur dioxide (Esposito, 1984). Venus measurements of sulfur dioxide acquired by the Pioneer mission were 10 times greater than the concentrations measured from Earth in the late 1950s suggesting a recent episode of volcanic activity. On Earth, sulfur compounds do not stay in the atmosphere for long. Instead, they react with the surface of the planet. The same is thought to be true at Venus, although the reactions are much slower. New observations from Venus Express showing rapid variations of sulfur dioxide in the upper atmosphere have revived this debate (Yung et al., 2009).

Finally, thermal IR measurements made by the VIRTIS instrument on Venus Express, show emissivity variations over the surface (Helbert et al., 2009; Smrekar et al., 2010). After correction for cloud transmittance and topography, the emissivity variations correlate to some extent with major geomorphic provinces such as corona and some “hotspot” volcanoes (Smrekar et al., 2010). Areas such as Idunn Mons and Imdr Regio have exceptionally high emissivity on their summits consistent with geologically recent volcanism (2500 yr to 2.5 Myr). Additional measurements are needed to narrow this age range for the most recent volcanism.

As mentioned before, three approaches can be used to detect volcanic activity on Venus; analysis of temporal variation in radar backscatter; temporal decorrelation; and InSAR phase change. Due to the current difficulty in predicting the level of atmospheric artifacts in the repeat-pass phase observations, amplitude variation and temporal decorrelation techniques have the highest chance of succeeding in robust change detection. While detecting surface activity-related change on Venus is unlikely within the limited lifetime of a satellite mission, an actual detection of such change would revolutionize our understanding of terrestrial planets.

There is a number of volcanic targets on Venus whose radiometric and structural characteristics suggest recent volcanism, warranting extensive analysis with change detection techniques. Such targets include the previously mentioned Maat Mons (2.1°N, 194.3°E), whose higher emissivity on the summit as well as the existence of summit domes instead of a caldera suggest recent volcanism (Robinson and Wood, 1993). Mylitta Fluctus (58°S, 351°E) appears to be a young, large (~800 km N-S and 380 km E-W) flow field where both radar-smooth and radar-rough lava flows have been identified (Roberts et al., 1992). Other interesting targets where surface activity might be expected (if it were to occur at all) include Beta Regio (25.3°N, 282.8°E) with its volcanoes Rhea and Theia Montes, Bell Regio (24–34°N, 40–55°E) where Tepev Mons is located, and Eistla Regio (12–30°N, 347° to 4°E), where Gula and Sif Montes are located.

3.3. Studying atmospheric turbulence

Although some observations on the structure and dynamics of the Venus atmosphere exist (e.g., Izakov, 2007; Woo et al., 1980) and a limited number of atmospheric models are available (Duan et al., 2010), the turbulence behavior of the Venus atmosphere at the spatial scales of interest for InSAR (below 50 km) is not well understood. Studying the structure, composition, and dynamics of the Venus atmosphere is the key mission goal of Venus Express (Svedhem et al., 2007), the first European mission to Venus, highlighting the limited amount of knowledge that exists today.

By utilizing the diverse observation parameters provided by a combination of repeat-pass and pass-to-pass InSAR acquisitions, an InSAR mission to Venus could answer some key questions about turbulence patterns in the Venus atmosphere. Due to the small offset of consecutive orbits, especially at higher latitudes, observations from several consecutive orbits can be combined to interferograms with temporal baselines of $n \times T_s$ (e.g., 100 min, 200 min, ...). After compensation for topographic phase effects using the InSAR-derived DEM from the first mapping cycle, the phase patterns in these interferograms can be analyzed to understand atmospheric turbulence in both the spatial and temporal domain. Due to the global acquisition principle, turbulence signatures can be compared for the day and night-side of the planet. Due to the limited spatial coverage of the SAR swath, mostly small scale turbulence patterns would be analyzed. The information gathered from such analyses may provide valuable input both for studies of the Venus atmosphere and for the quantification of atmospheric effects on amplitude, phase, and coherence of SAR and InSAR observations.

4. Conclusions and recommendations

Repeat pass interferometry is a proven technology that relies on 4 constraints. (1) The radar must provide phase-preserving imagery. (2) The scatterers on the imaged surface cannot change significantly between the reference and repeat observations. (3) The reference and repeat orbits need to be controlled to an accuracy of better than say 1000 m to achieve good interferograms. (4) The post data collection orbits must be highly accurate since the slope of the orbital error will map directly into the slope of the topography being recovered.

A major advantage of repeat-pass InSAR on Venus with respect to the Earth is that the lack of vegetation and erosional processes will result in very high interferometric coherence, which will facilitate automated phase recovery and unwrapping. The main disadvantages of InSAR on Venus with respect to Earth are that the orbital control and knowledge will not be as accurate because of incomplete tracking data. Several areas of our study demonstrate a direct link between better orbit control and lower radar bandwidth. One of the main mission bottlenecks is the ability to downlink the SAR data back to Earth at the full resolution needed for InSAR. Given a fixed rate of data transmission back to Earth, orbit control will map directly into increased surface coverage because of the lower radar bandwidth needed. Although the range resolution is dependent on the radar bandwidth, the accuracy and resolution of the derived topography does meet the goals for all considered bandwidth scenarios. Therefore given robust and thoroughly tested radar, the main challenge of this mission will be improving the real-time orbit control to the sub-kilometer accuracy.

Two types of InSAR scenarios – repeat-pass and pass-to-pass InSAR – were proposed in this study that both achieve complementary products of topography and surface change. Careful mixing of these two modes could lead to an optimized mission with early science payoff and continued possibility for discovery during the mission lifetime. *Mode 1*: The slow rotation rate of Venus offers the possibility of pass-to-pass interferometry since the horizontal distance between orbits is only 11 km at the equator (assuming a near circular orbit at 600 km altitude). In this mode, a 22 km wide radar swath would be collected during the first orbit. For every odd numbered orbit, a similar swath would be collected but the radar frequency would be offset to accommodate the spectral shift due to the slight changes of look angle and which surface features are observed. This scenario has been tested on the Earth resulting in interferograms having spectacular vertical topography resolution of 0.5 m. In this mode

the best results are achieved in areas of relatively flat topography. Therefore, this mode is optimal for science targets of comparably low relief. *Mode 2* is the standard repeat-pass InSAR: The swaths acquired during the first Venus day would be re-acquired along repeat orbits controlled within about 1/4 of the critical baseline. A radar bandwidth as low as 15 MHz could be used for this scenario as long as the repeat-orbit was well navigated. Similar data could be collected during the third Venus day. Given the characteristics of the radar, there are no cases where high quality InSAR data cannot be collected. The issue is data coverage; maximum data coverage will rely on good orbit control and a well-designed operation scenario.

Acknowledgments

Peter Mouginnis-Mark, Robert Herrick, Catherine Johnson, Remko Scharroo, Ford Rogers, Bob Grim, and Buck Sharpton all contributed to discussions related to InSAR mapping on Venus. This research was partly supported by the National Science Foundation (EAR 0811772) and NASA (NNX09AD12G).

Appendix A

A1. Principles and conditions of SAR interferometry

Every element of a complex SAR data set contains two types of information, the signal's amplitude A and its respective phase ψ . The signal amplitude is a measure of the amount of energy reflected back to the radar and is a function of the roughness of the observed surface, the orientation of the surface with respect to the look direction of the radar, and the dielectric properties of the material. The signal phase ψ , modulo 2π , is a measure of the two-way distance from the spacecraft to a reflector on the ground. Since the distance and reflective properties of each pixel vary, the phase of an individual SAR image is essentially a random function of position. However, if two images are acquired from almost identical vantage points and nothing has disturbed the reflective properties of the surface, then the phase difference ϕ between the two images will reveal information about surface topography and surface deformation. To extract ϕ , a so called *interferogram* I is formed through cross multiplication of two co-registered complex SAR images C_1 and C_2

$$I = C_1 C_2^* = A_1 A_2 e^{j(\psi_1 - \psi_2)} \quad (\text{A} - 1)$$

where $e^{j\psi}$ is the exponential function, and j is the imaginary unit. The *interferometric phase* ϕ can then be extracted from the complex interferogram through $\phi = \arg(I)$.

The interferometric phase ϕ can be seen as a linear combination of the following contributions

$$\phi = \phi_{\text{surface}} + \phi_{\text{topo}} + \phi_{\text{defo}} + \phi_{\text{iono}} + \phi_{\text{tropo}} + \phi_{\text{orbit}} + \phi_{\text{noise}} \quad (\text{A} - 2)$$

where ϕ_{surface} is caused by the curvature of a planet's surface, ϕ_{topo} is due to surface topography, ϕ_{defo} represents surface deformation, ϕ_{iono} and ϕ_{tropo} are propagation delays in ionosphere and troposphere, while ϕ_{orbit} and ϕ_{noise} are contributions from orbit uncertainties and system noise. The phase components ϕ_{surface} and ϕ_{topo} scale with the across-track distance between the orbit tracks of acquisitions 1 and 2, usually called *interferometric baseline* B . For a comprehensive review of InSAR methodology and applications, the reader is referred to the review papers of Rosen et al. (2000) and Bamler and Hartl (1998).

For InSAR at Venus, the largest contribution of Eq. (A-2) is the phase due to the curvature of the planet. With an accurate orbit, this contribution can be removed from the interferogram using a model of a spherical surface of constant radius. For a mission to

Venus we would be most interested in the phase contributions from both topography and surface deformation. They can be separated by adjusting the length of the perpendicular baseline as shown in Fig. A1. A longer baseline results in a higher sensitivity to topography while a shorter or zero baseline is best for detecting surface deformation. Since the baseline cannot be controlled to be zero, the strategy is to first form an interferogram from a longer baseline pair to determine the topographic phase and then remove this topographic phase from the shorter baseline pair to determine the surface deformation. Thus a minimum of two SAR images are needed for recovery of topography and a minimum of three images are needed to measure deformation. Fig A2 shows an example of amplitude and phase of an interferogram showing surface deformation caused by the 1999 Hector Mine Earthquake. White dashed lines show the zone of the surface rupture. Each fringe represents 28 mm of line-of-sight (LOS) motion toward the spacecraft.

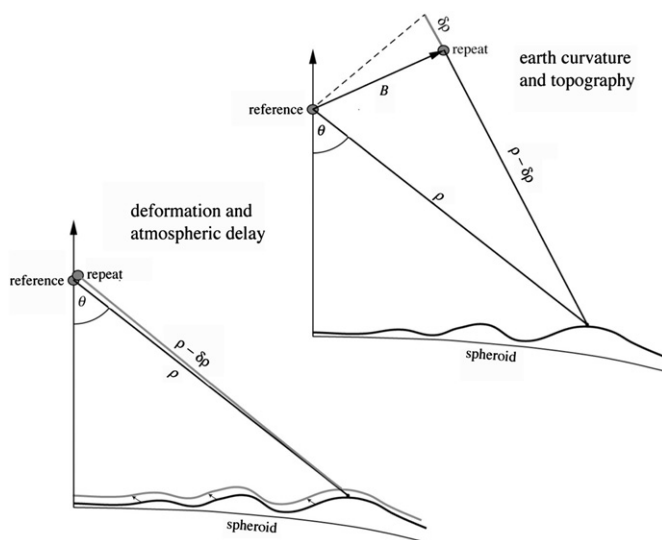


Fig. A1. (Left) end view of reference and repeat tracks where baseline is small shows sensitivity to surface deformation and atmospheric delay. (Right) end view of reference and repeat tracks for larger baseline shows sensitivity to earth curvature and surface topography.

A1.1. Conditions for SAR interferometry

For SAR interferometry observations to yield useful information, coherent observation conditions are required. From a signal processing perspective, the signals acquired by two observations are only coherent if they sample overlapping parts of the ground reflectivity (or object) spectrum (see Fig. A3), or in other words, if they observe the same spectral characteristics of the observed surface. Shifts between the observed spectra are caused by differences in the three-dimensional observation geometry, specifically by differences in the incidence angle with which a point on ground is observed (see Sections A1.1.1) and by differences of squint angles during the observation of the interferometric partner images (see Sections A1.1.2).

A1.1.1. Interferometric baseline and spectral shifts. Spectral shifts in SAR images originate from the difference between the object spectrum of an observed surface and the SAR signal spectrum as shown in Fig. A3. The object spectrum is a function of the object properties (e.g., radar reflectivity of the surface) and is independent of the imaging characteristics. The SAR signal spectrum is the segment of the object spectrum that is observed by an imaging system and is therefore dependent on its specifications, foremost its bandwidth, sampling frequency, and observation geometry.

In (across-track) interferometry, two images observing the ground from slightly different across-track locations are combined to form an interferogram. Due to their difference in observation geometry, expressed by different look angles θ_1 and θ_2 , a slightly different section of the object spectrum will be mapped into the respective observed signal spectra (see Fig. A3). The size of the relative spectral shift between the observed object spectra depends on the look angle difference, expressed by the length of the effective baseline $B_{\perp, \text{effective}}$, the local surface slopes α , the wavelength of the system λ , and the range to the object on the ground ρ , and can be calculated from

$$\Delta f(\alpha) = -\frac{c \times B_{\perp, \text{effective}}}{\rho \lambda \tan(\theta - \alpha)} \quad (\text{A} - 3)$$

The shift between the observed object spectra causes the two images to have an overlapping spectral part, which contains information, and two non-overlapping parts, which can be considered as noise in an interferogram (cf. Fig. A3B). Therefore, a

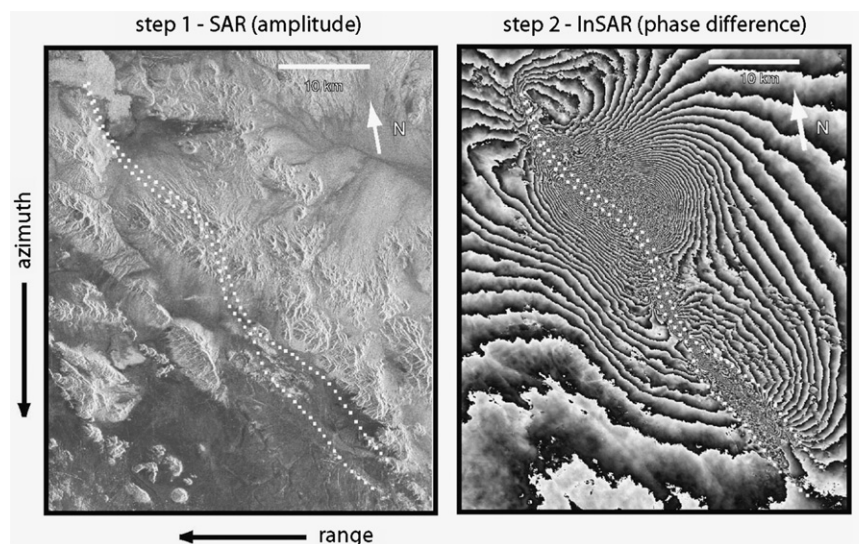


Fig. A2. Images of amplitude (left) and phase difference (right) for ERS SAR data spanning the 1999 Hector Mine Earthquake. White squares show the zone of the surface rupture. Each fringe represents 28 mm of line-of-sight (LOS) motion toward the spacecraft.

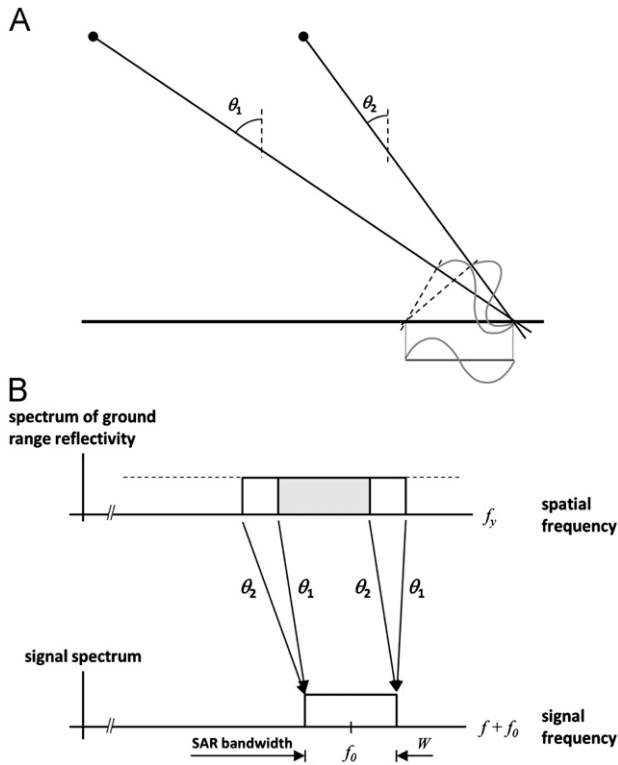


Fig. A3. Mapping of ground range reflectivity (object spectrum) to the frequency domain in the SAR signal spectrum. (A) mapping of the object spectrum onto the signal spectra of two acquisitions with different geometry, causing the same object frequency to appear shifted in the two SAR signal spectra. (B) Frequency shift in range caused by the different look angles.

bandpass filter is needed to eliminate the non-overlapping components. To tune the bandpass filter it is necessary to know $\Delta f(\alpha)$ as accurately as possible, requiring accurate knowledge of baseline, look angle, and local surface slopes.

As the spectral shift increases with baseline length, and as the bandwidth W of a SAR system is limited, there is a maximum baseline length, called *critical baseline* $B_{\perp,crit}$ for which interferometry is still possible. The critical baseline is the baseline for which $\Delta f(\alpha) = W$ and can be calculated from

$$B_{\perp,crit} = -\frac{W\rho\lambda\tan(\theta-\alpha)}{c} \quad (A-4)$$

For topographic recovery, a baseline of about 1/4 of the critical value is generally considered optimal. Increasing the critical baseline can be achieved by either increasing the system's range bandwidth W or by tuning the signal spectrum of the second acquisition such that the average spectral shift is absorbed (Gatelli et al., 1994).

After non-overlapping spectral components have been removed through bandpass filtering, the effective range bandwidth has been reduced yielding a reduced range resolution given by

$$\Delta\rho_{range}(\alpha) = \frac{c}{2(W-\Delta f(\alpha))} \quad (A-5)$$

Keeping the perpendicular baseline below the critical baseline is required for recovery of interferometric phase information.

A1.1.2. Spectral shifts in azimuth direction. Preserving the phase coherence in InSAR additionally requires sufficiently overlapping azimuth Doppler spectra. The Doppler bandwidth depends on the satellite orbit, the satellite attitude, and the antenna length and is typically within 2000–4000 Hz. The width of the Doppler

spectrum defines the required pulse repetition frequency (PRF) of the radar, which has to be selected slightly higher than the Doppler bandwidth to warrant sufficient data sampling. Assuming unweighted spectra, the properties of the Doppler spectrum of SAR image k can be expressed by its Doppler centroid frequency $f_{DC,k}$ and its Doppler (or azimuth) bandwidth $W_{az,k}$. Differences in f_{DC} between two interferometric partners can be caused by (i) different squint angles of the sensors, or (ii) non-parallelity of the respective orbits.

The antenna of a SAR system is generally aimed almost perpendicular to the sum of the flight direction vector and the velocity vector due to the planet's rotation. Nevertheless, there will always be a slight *squint angle* ϕ_s of the spacecraft, steering the antenna away from the zero-Doppler direction. This causes a shift of the Doppler centroid frequency corresponding to

$$\Delta f_{DC}(\phi_s) = \frac{2v_{s/c}}{\lambda} \sin(\phi_s) \quad (A-6)$$

where $v_{s/c}$ is the velocity of the spacecraft in an earth- or Venus-fixed frame.

Non-parallelity of orbits can be expressed by an orbit convergence with a perpendicular velocity v_{\perp} . This convergence causes a Doppler shift according to

$$\Delta f_{DC}(v_{\perp}) = \frac{2v_{\perp}}{\lambda} \quad (A-7)$$

If the Doppler centroids of interferometric partners are not identical, bandpass azimuth filtering can be performed to remove non-overlapping parts of the Doppler spectra and maximize interferometric coherence.

References

- Bamler, R., Hartl, P., 1998. Synthetic aperture radar interferometry. *Inverse Problems* 14 (4), R1–R54.
- Bilotti, F., Suppe, J., 1999. The global distribution of wrinkle ridges on Venus. *Icarus* 139 (1), 137–157.
- Carter, L.M., Campbell, D.B., Margot, J.L., and Campbell, B.A. Mapping the topography of Maxwell montes using ground-based radar interferometry. In: *Proceedings 37th Annual Lunar and Planetary Science Conference*, League City, Texas, 2006, 37, p. abstract no. 2261.
- Chlieh, M., de Chabaliere, J.B., Ruegg, J.C., Armijo, R., Mowska, R., Campos, J., Feigl, K.L., 2004. Crustal deformation and fault slip during the seismic cycle in the North Chile subduction zone, from GPS and InSAR observations. *Geophysical Journal International* 158 (2), 695–711.
- Crisp, D., Allen, M., Anicich, V., Arvidson, R., Atreya, S., Baines, K., Banerdt, W., Bjoraker, G., Bougher, S., and Campbell, B., 2002. Divergent evolution among earth-like planets: the case for Venus exploration: the future of solar system exploration (2003–2013)—community contributions to the NRC solar system exploration decadal survey. *ASP Conference Proceedings*, 272, pp. 5–34.
- Crisp, D., Titov, D.V., 1997. The thermal balance of the Venus atmosphere. In: Bougher, S.W., Hunten, D.M., Phillips, R.J. (Eds.), *Venus II: University of Arizona*. University of Arizona Press, Tucson, AZ, pp. 353–384.
- Dieterich, J., 1994. A constitutive law for rate of earthquake production and its application to earthquake clustering. *Journal of Geophysical Research* 99, 2601–2601.
- Duan, X., Moghaddam, M., Wenkert, D., Jordan, R.L., Smrekar, S.E., 2010. X band model of Venus atmosphere permittivity. *Radio Science* 45 (2), RS2003.
- Emardson, T.R., Simons, M., Webb, F.H., 2003. Neutral atmospheric delay in interferometric synthetic aperture radar applications: Statistical description and mitigation. *Journal of Geophysical Research* 108 (B5), 2231.
- Espósito, L.W., 1984. Sulfur dioxide: episodic injection shows evidence for active Venus volcanism. *Science* 223 (4640), 1072–1074.
- Farr, T.G., Rosen, P.A., Caro, E., Crippen, R., Duren, R., Hensley, S., Kobrick, M., Paller, M., Rodriguez, E., Roth, L., Seal, D., Shaffer, S., Shimada, J., Umland, J., Werner, M., Oskin, M., Burbank, D., Alsdorf, D., 2007. The shuttle radar topography mission. *Reviews of Geophysics* 45 (2), RG2004.
- Ferretti, A., Prati, C., Rocca, F., 2000. Nonlinear subsidence rate estimation using permanent scatterers in differential SAR interferometry. *IEEE Transactions on Geoscience and Remote Sensing* 38 (5), 2202–2212.
- Ferretti, A., Prati, C., Rocca, F., 2001. Permanent scatterers in SAR interferometry. *IEEE Transactions on Geoscience and Remote Sensing* 39 (1), 8–20.
- Fielding, E.J., Blom, R.G., Goldstein, R.M., 1998. Rapid subsidence over oil fields measured by SAR interferometry. *Geophysical Research Letters* 25 (17), 3215–3218.

- Ford, P.G., Pettengill, G.H., 1992. Venus topography and kilometer scale slopes. *Journal of Geophysical Research-Planets* 97 (E8), 13103–13114.
- Gatelli, F., Guamieri, A.M., Parizzi, F., Pasquali, P., Prati, C., Rocca, F., 1994. The wavenumber shift in SAR interferometry. *IEEE Transactions on Geoscience and Remote Sensing* 32 (4), 855–865.
- Ghail, R., Wilson, C., Galand, M., Hall, D., Cochran, C., Mason, P., Helbert, J., MontMessin, F., Limaye, S., Patel, M., Bowles, N., Stam, D., Wählund, J.-E., Rocca, F., Waltham, D., Mather, T., Biggs, J., Genge, M., Paillou, P., Mitchell, K., Wilson, L., Singh, U., 2012. EnVision: taking the pulse of our twin planet. *Experimental Astronomy* 33 (2), 337–363.
- Gierasch, P.J., Yung, Y.L., 2002. Planetary atmospheres: Venus. In: Holton, J.R., Pyle, J., Curry, J.A. (Eds.), *Encyclopedia of Atmospheric Sciences*. Academic Press, pp. 1755–1760.
- Gong, W., Meyer, F., Webley, P.W., Morton, D., and Liu, S., Performance analysis of atmospheric correction in InSAR data based on the weather research and forecasting model (WRF). In: *Proceedings Geoscience and Remote Sensing Symposium (IGARSS)*, 2010 IEEE International, Honolulu, Hawaii, 25–30 July 2010 2010, pp. 2900–2903.
- Gonzalez, J.H., Bachmann, M., Krieger, G., Fiedler, H., 2010. Development of the TanDEM-X calibration concept: analysis of systematic errors. *IEEE Transactions on Geoscience and Remote Sensing* 48 (2), 716–726.
- Greeley, R., Arvidson, R.E., Elachi, C., Geringer, M.A., Plaut, J.J., Saunders, R.S., Schubert, G., Stofan, E.R., Thouvenot, E.J.P., Wall, S.D., Weitz, C.M., 1992. Aeolian features on Venus: preliminary Magellan results. *Journal of Geophysical Research* 97 (E8), 13319–13345.
- Grosfils, E.B., Head, J.W., 1996. The timing of giant radiating dike swarm emplacement on Venus: implications for resurfacing of the planet and its subsequent evolution. *Journal of Geophysical Research* 101 (E2), 4645–4656.
- Hansen, R., 2001. *Radar Interferometry: Data Interpretation and Error Analysis*. Kluwer Academic Publishers.
- Helbert, J., Mueller, N., Maturilli, A., Piccioni, G., and Drossart, P., 2009. The long and Hot Way from Brightness Anomalies to Compositional Information—High Temperature Laboratory Spectroscopy for VIRTIS on Venus Express, 40th Lunar and Planetary Science Conference: The Woodlands, Texas.
- Hensley, S., and Shaffer, S., Repeat pass radar observations of Venus from the Magellan radar system. In: *Proceedings 41st Lunar and Planetary Science Conference*, The Woodlands, Texas, 2010, 41, p. 2369.
- Herrick, R.R., Stahlke, D.L., Sharpton, V.L., 2012. Fine-scale Venusian topography from Magellan stereo data. *Eos, Transactions, American Geophysical Union* 93 (12).
- Hoffmann, J., Zebker, H.A., Galloway, D.L., Amelung, F., 2001. Seasonal subsidence and rebound in Las Vegas Valley, Nevada, observed by synthetic aperture radar interferometry. *Water Resources Research* 37 (6), 1551–1566.
- Izakov, M., 2007. Turbulence in the free atmospheres of Earth, Mars, and Venus: a review. *Solar System Research* 41 (5), 355–384.
- Just, D., Bamler, R., 1994. Phase statistics of interferograms with applications to synthetic-aperture radar. *Applied Optics* 33 (20), 4361–4368.
- Kenji, L.W., Kaufmann, V., 2003. Estimation of rock glacier surface deformation using SAR interferometry data. *IEEE Transactions on Geoscience and Remote Sensing* 41 (6), 1512–1515.
- Klose, K.B., Wood, J.A., Hashimoto, A., 1992. Mineral equilibria and the high radar reflectivity of Venus mountaintops. *Journal of Geophysical Research* 97 (E10), 16353–16369.
- Kreslavsky, M.A., Basilevsky, A.T., 1998. Morphometry of wrinkle ridges on Venus: comparison with other planets. *Journal of Geophysical Research* 103 (E5), 11103–11111.
- Krieger, G., Moreira, A., Fiedler, H., Hajnsek, I., Werner, M., Younis, M., Zink, M., 2007. TanDEM-X: a Satellite formation for high-resolution SAR interferometry. *IEEE Transactions on Geoscience and Remote Sensing* 45 (11), 3317–3341.
- Markiewicz, W.J., Titov, D.V., Limaye, S.S., Keller, H.U., Ignatiev, N., Jaumann, R., Thomas, N., Michalik, H., Moissl, R., Russo, P., 2007. Morphology and dynamics of the upper cloud layer of Venus. *Nature* 450 (7170), 633–636.
- Massonnet, D., Feigl, K.L., 1998. Radar interferometry and its application to changes in the Earth's surface. *Reviews of Geophysics* 36, 441–500.
- Meyer, F., Bamler, R., Leinweber, R., and Fischer, J. A comparative analysis of tropospheric water vapor measurements from MERIS and SAR. In: *Proceedings Geoscience and Remote Sensing Symposium*, 2008. IGARSS 2008. IEEE International 2008, 4, pp. IV – 228–IV – 231.
- Meyer, F., Gernhardt, S., and Adam, N. Long-term and seasonal subsidence rates in Urban Areas from Persistent Scatterer Interferometry. In: *Proceedings Urban Remote Sensing Joint Event*, 2007 2007, pp. 1–6.
- Meyer, F.J., 2007. Topography and displacement of polar glaciers from multi-temporal SAR interferograms. *Polar Record* 43 (227), 331–343.
- Phillips, R.J., Arvidson, R.E., Boyce, J.M., Campbell, D.B., Guest, J.E., Schaber, G.G., Soderblom, L.A., 1991. Impact craters on Venus: initial analysis from Magellan. *Science* 252 (5003), 288–297.
- Poland, M., Miklius, A., Orr, T., Sutton, J., Thornber, C., Wilson, C., Hui, D., Luo, Y., Schimmel, D., Clark, J., 2008. New episodes of volcanism at Kilauea Volcano, Hawaii. *Eos* 89 (5), 37–38.
- Rignot, E., Bamber, J.L., Van den Broeke, M.R., Davis, C., Li, Y., Van de Berg, W.J., Van Meijgaard, E., 2008. Recent Antarctic ice mass loss from radar interferometry and regional climate modelling. *Nature Geoscience* 1 (2), 106–110.
- Rignot, E., Gogineni, S., Joughin, I., Krabill, W., 2001. Contribution to the glaciology of northern Greenland from satellite radar interferometry. *Journal of Geophysical Research-Atmospheres* 106 (D24), 34007–34019.
- Rignot, E., Vaughan, D.G., Schmeltz, M., Dupont, T., MacAyeal, D., 2002. Acceleration of Pine Island and Thwaites Glaciers, West Antarctica. *Annals of Glaciology* 34 (1), 189–194.
- Roberts, K.M., Guest, J.E., Head, J.W., Lancaster, M.G., 1992. Mylitta Fluctus, Venus: rift-related, centralized volcanism and the emplacement of large-volume flow units. *Journal of Geophysical Research* 97 (E10), 15991–16015.
- Robinson, C.A., Wood, J.A., 1993. Recent volcanic activity on Venus: evidence from radiothermal emissivity measurements. *Icarus* 102 (1), 26–39.
- Rosen, P.A., Hensley, S., Joughin, I.R., Li, F.K., Madsen, S.N., Rodriguez, E., Goldstein, R.M., 2000. Synthetic aperture radar interferometry. *Proceedings of the IEEE* 88 (3), 333–382.
- Roth, L.E., Wall, S.D., 1995. *The Face of Venus. The Magellan Radar-Mapping Mission*. NASA Special Publication SP-520, Washington, DC.
- Rowland, S.K., Smith, G.A., Mouginiis-Mark, P.J., 1994. Preliminary ERS-1 observations of Alaskan and Aleutian volcanoes. *Remote Sensing of Environment* 48 (3), 358–369.
- Ryder, I., Parsons, B., Wright, T.J., Funning, G.J., 2007. Post-seismic motion following the 1997 Manyi (Tibet) earthquake: InSAR observations and modeling. *Geophysical Journal International* 169 (3), 1009–1027.
- Sandwell, D., Myer, D., Shimada, M., Brooks, B., and Foster, J. Vector deformation maps of the father's day intrusion at Kilauea: constraints on magma injection. In: *Proceedings American Geophysical Union, Fall Meeting 2007*, San Francisco, CA, 2007, p. Abstract V53A-1136.
- Srekar, S.E., Stofan, E.R., Mueller, N., Treiman, A., Elkins-Tanton, L., Helbert, J., Piccioni, G., Drossart, P., 2010. Recent hotspot volcanism on Venus from VIRTIS emissivity data. *Science* 328 (5978), 605–608.
- Solomon, S.C., 1993. The geophysics of Venus. *Physics Today* 46, 48–55.
- Stramondo, S., Bozzano, F., Marra, F., Wegmüller, U., Cinti, F.R., Moro, M., Saroli, M., 2008. Subsidence induced by urbanisation in the city of Rome detected by advanced InSAR technique and geotechnical investigations. *Remote Sensing of Environment* 112 (6), 3160–3172.
- Strozzi, T., Kouraev, A., Wiesmann, A., Wegmüller, U., Sharov, A., Werner, C., 2008. Estimation of Arctic glacier motion with satellite L-band SAR data. *Remote Sensing of Environment* 112 (3), 636–645.
- Suzuki, S., Osawa, Y., Hatooka, Y., Kankaku, Y., and Watanabe, T., Overview of Japan's Advanced Land Observing Satellite-2 mission. In: *Proceedings Proc. SPIE 7474*, 74740Q Berlin, Germany, 2009.
- Svedhem, H., Titov, D.V., McCoy, D., Lebreton, J.P., Barabash, S., Bertaux, J.L., Drossart, P., Formisano, V., Häusler, B., Korabely, O., Markiewicz, W.J., Nevejans, D., Pätzold, M., Piccioni, G., Zhang, T.L., Taylor, F.W., Lellouch, E., Koschny, D., Witasse, O., Eggel, H., Warhaut, M., Acomazzo, A., Rodriguez-Canabal, J., Fabrega, J., Schirmann, T., Clochet, A., Coradini, M., 2007. Venus express—the first European mission to Venus. *Planetary and Space Science* 55 (12), 1636–1652.
- Teatini, P., Tosi, L., Strozzi, T., Carbognin, L., Cecconi, G., Rosselli, R., Libardo, S., 2012. Resolving land subsidence within the Venice Lagoon by persistent scatterer SAR interferometry. *Physics and Chemistry of the Earth, Parts A/B/C* 40–41, 72–79.
- Turcotte, D.L., 1993. An episodic hypothesis for Venusian tectonics. *Journal of Geophysical Research* 98 (E9), 17061–17068.
- Verner, K.R., Galgana, G.A., McGovern, P.J., and Herrick, R.R., 2011. Insights into the structure and evolution of large volcanoes on Venus from high-resolution stereo-derived topography. 42nd Lunar and Planetary Science Conference: The Woodlands, TX, p. 2712.
- VEXAG, 2007. *Venus Scientific Goals, Objectives, Investigations, and Priorities: 2007*.
- Wegmüller, U., Santoro, M., Werner, C., Strozzi, T., and Wiesmann, A. ERS-ENVISAT Tandem cross-interferometry coherence estimation. In: *Proceedings Geoscience and Remote Sensing Symposium*, 2009 IEEE International, IGARSS 2009 12–17 July 2009 2009, Volume 1, p. 1-128-1-131.
- Wegmüller, U., Santoro, M., Werner, C., Strozzi, T., Wiesmann, A., Lengert, W., 2009. DEM generation using ERS-ENVISAT interferometry. *Journal of Applied Geophysics* 69 (1), 51–58.
- Wei, M., Sandwell, D., Smith-Konter, B., 2010. Optimal combination of InSAR and GPS for measuring interseismic crustal deformation. *Advances in Space Research* 46 (2), 236–249.
- Woo, R., Armstrong, J.W., Ishimaru, A., 1980. Radio occultation measurements of turbulence in the Venus atmosphere by Pioneer Venus. *Journal of Geophysical Research* 85 (A13), 8031–8038.
- Wright, T.J., Lu, Z., Wicks, C., 2003. Source model for the M-w 6.7, 23 October 2002, Nenana Mountain Earthquake (Alaska) from InSAR. *Geophysical Research Letters* 30 (18), p.
- Yung, Y.L., Liang, M.C., Jiang, X., Shia, R.L., Lee, C., Bézard, B., Marcq, E., 2009. Evidence for carbonyl sulfide (OCS) conversion to CO in the lower atmosphere of Venus. *Journal of Geophysical Research* 114 (E5), E00B34.
- Zebker, H.A., Farr, T.G., Salazar, R.P., Dixon, T.H., 1994. Mapping the world's topography using radar interferometry: the TOPSAT mission. *Proceedings of the IEEE* 82 (12), 1774–1786.
- Zebker, H.A., Goldstein, R.M., 1986. Topographic mapping from interferometric synthetic aperture radar observations. *Journal of Geophysical Research* 91 (B5), 4993–4999.
- Zebker, H.A., Rosen, P., Hensley, S., Mouginiis-Mark, P.J., 1996. Analysis of active lava flows on Kilauea volcano, Hawaii, using SIR-C radar correlation measurements. *Geology* 24 (6), 495–498.